Materials Today Bio 26 (2024) 101104

Contents lists available at ScienceDirect

Materials Today Bio

journal homepage: www.journals.elsevier.com/materials-today-bio

Turning sublimed sulfur and bFGF into a nanocomposite to accelerate wound healing via co-activate FGFR and Hippo signaling pathway

Jieqiong Cao [a,b,1], Zijian Su [b,1], Yibo Zhang [b,1], Zhiqi Chen [b], Jingsheng Li [b], Yulin Cai [b], Yiming Chang [a], Minghua Lei [b], Qianyi He [b], Weicai Li [b], Xuan Liao [c], Shuixing Zhang [a,***], An Hong [a,b,**], Xiaojia Chen [a,b,*]

[a] Department of Radiology, The First Affiliated Hospital of Jinan University, Guangzhou, China
[b] Department of Cell Biology & Institute of Biomedicine, College of Life Science and Technology, State Key Laboratory of Bioactive Molecules and Druggability Assessment, Jinan University, Guangdong Province Key Laboratory of Bioengineering Medicine, Guangdong Provincial Biotechnology Drug & Engineering Technology Research Center, National Engineering Research Center of Genetic Medicine, Guangzhou, China
[c] Department of Plastic Surgery, The First Affiliated Hospital of Jinan University, Guangzhou, China

ARTICLE INFO

Keywords:
Nanocomposite
Diabetic wound healing
FGFR pathway
Hippo pathway

ABSTRACT

Clinical treatment of diabetic refractory ulcers is impeded by chronic inflammation and cell dysfunction associated with wound healing. The significant clinical application of bFGF in wound healing is limited by its instability *in vivo*. Sulfur has been applied for the treatment of skin diseases in the clinic for antibiosis. We previously found that sulfur incorporation improves the ability of selenium nanoparticles to accelerate wound healing, yet the toxicity of selenium still poses a risk for its clinical application. To obtain materials with high pro-regeneration activity and low toxicity, we explored the mechanism by which selenium-sulfur nanoparticles aid in wound healing via RNA-Seq and designed a nanoparticle called Nano-S@bFGF, which was constructed from sulfur and bFGF. As expected, Nano-S@bFGF not only regenerated zebrafish tail fins and promoted skin wound healing but also promoted skin repair in diabetic mice with a profitable safety profile. Mechanistically, Nano-S@bFGF successfully coactivated the FGFR and Hippo signalling pathways to regulate wound healing. Briefly, the Nano-S@bFGF reported here provides an efficient and feasible method for the synthesis of bioactive nanosulfur and bFGF. In the long term, our results reinvigorated efforts to discover more peculiar unique biofunctions of sulfur and bFGF in a great variety of human diseases.

1. Introduction

Skin wound closure is a highly accurate and finely ordered process in a healthy individuals [1]. Nevertheless, shortcomings in this process have lead to approximately 305 million chronic wound patients worldwide, with diabetes as an important factor leading to delayed wound healing and amputation [2], causing a considerable economic impact on health care systems and, ultimately, on the country's economy. Despite these high costs, two key issues persist that impede the healing process, resulting in poor repair efficacy:1) wound healing requires multiple signalling pathways to regulate a variety of cell activities [3–5], and no active molecule can regulate multiple signalling pathways resulting in poor wound repair; 2) long-term inflammation due to infection seriously limits the healing of diabetic wounds [6]. Although there are a variety of wound healing treatments, especially these biomaterials [7–9] and wound dressings [10,11], a comprehensive therapeutic strategy involving regulating various cell activities and inducing of macrophage polarization for wound healing is urgently needed for the chronic wounds.

Sulfur (S), a classic of oxygen group element that possesses electronic, antioxidant [12], and antibacterial [13] properties, has been widely used for a variety of dermatological treatments, including wound healing [14], skin rash treatment [15] and psoriasis treatment [16]. Despite the high activity of S, direct application to the skin results in low

* Corresponding author.
** Corresponding author.
*** Corresponding author.
E-mail addresses: shui7515@126.com (S. Zhang), tha@jnu.edu.cn (A. Hong), tchenxj@jnu.edu.cn (X. Chen).
[1] Jieqiong Cao, Zijian Su and Yibo Zhang have contributed equally to this work.

https://doi.org/10.1016/j.mtbio.2024.101104
Received 8 March 2024; Received in revised form 17 May 2024; Accepted 27 May 2024
Available online 27 May 2024

bioactivity due to the presence of a skin barrier, and S nanoparticles are considered the most active and effective form [17,18]. Recently, our group reported that the use of selenium nanoparticles (Nano-Se) mixed with S to construct selenium-sulfur nanocomposite particles (Nano--Se@S) significantly accelerated the effect of Nano-Se on wound repair by regulating the functions of a variety of regeneration-related cells [19]. However, two key issues limit the application of Nano-Se@S in wound healing: 1) the mechanism of S in wound healing is still unclear and the efficacy of S in the repair of diabetic refractory wounds has not been reported. 2) The cumulative toxicity of Se might be a potential limitation for its application in wound healing, excessive intake of Se could cause toxic reactions, including but not limited to dyspnoea, tetanic spasms, and death from respiratory failure [20], and myocarditis [21]. Therefore, exploring the mechanisms of Se and S in Nano-Se@S and determining the ability of clinical drugs to replace Se for pro-regeneration activity is the key strategy to solve this problem.

Herein, transcriptome analysis was performed to explore the mechanisms by which Nano-Se@S stimulates the wound healing. Interestingly, we found that Nano-Se and Nano-S might promote wound healing through the FGFR and Hippo signalling pathways. Therefore, basic fibroblast growth factor (bFGF) was selected as an FGFR activator, and hydrosoluble Nano-S@bFGF was synthesized from bFGF, S and PEG200. Multiple cell models, zebrafish fin regeneration and a mice skin regeneration model were used to investigate the regeneration capacity of Nano-S@bFGF. Interestingly, within a safe dose range, Nano-S@bFGF not only regenerated zebrafish tail fins and mice skin but also promoted skin in diabetic mice through the FGFR and Hippo pathways. Our study highlighted the cooperation of S as a feasible approach for accessing synthetic bFGF-containing nanoparticles with reduced toxicity and broadened the application of nano-S in regenerative medicine.

2. Materials and methods

2.1. Materials

S (7704-34-9; >99 %), MS-222 (866-86-2) and bFGF (GF003; >98 %) were purchased from Sigma-Aldrich Chemical Co., PEG200 (25322-68-3; >99 %) was purchased from Sangon Biotech Co. Ltd. and used without further purification. AZD4547 (1035270-39-3; >99 %), Verteporfin (129497-78-5; >99 %) were purchased from MedChemExpress. CD86 (ab220188), CD163 ab316218, CD206 (ab8918), iNOS1 (ab49999), TNF-a (ab1793), Yap (ab56701), *p*-FGFR (ab59194) antibody were purchased from abcam. DMEM was purchased from Gibco Co. Ltd. FBS was purchased from Biological Industries Co. Ltd. The BeyoClick™ EdU Cell Proliferation Kit (C0071S) was purchased from Beyotime Biotechnology Co., Ltd. Ultrapure Milli-Q water was used in all experiments.

2.2. Cell lines

Cell lines, including human umbilical vein endothelial (HUVEC) and human skin fibroblast (HSF) were purchased from American Type Culture Collection (ATCC, Manassas, VA, USA).

2.3. Extraction and purification of total RNA from mice regenerated skin tissue and bioinformatics analysis

Four skin wounds were constructed on the back of each Balb/c mice, they were randomly divided into four groups: one group was cultured in system aquaculture (control group), Nano-S (8 ng/mL), Nano-Se (8 ng/mL) and Nano-Se@S (8 ng/mL) every other day for 8 days. Then, the regeneration tissue was collected. Total RNA was obtained with a RNeasy Micro Kit according to standard operating procedures. After electrophoresis, an RNA Clean XP Kit and RNase-Free DNase Set was used to purify total RNA. Only high-quality RNA samples (OD260/280 = 1.8–2.0, RIN ≥9.5, 28S:18S = 1.6–2.4) were used to construct a sequencing library, Illumina HiSeq X10 was used, and RNA purification was performed at Shanghai Bohao Biotechnology Co., Ltd. Reverse transcription, library construction, and sequencing were performed. For bioinformatics analysis, the expression level of each transcript was calculated based on the number of fragments per million exons per million mapped reads (FPKM) method. RSEM was used to quantify gene abundance. The R statistical software package DESeq2 (fold change≥2 and P value < 0.05) was used to identify differentially expressed genes with a false discovery rate (FDR) cut-off value < 0.05.

2.4. Synthesis and characterization of Nano-S@bFGF

Nano-S@bFGF was synthesized by dissolving 10 mg of S powder in 10 mL of PEG200 (>99 %) solution under magnetic stirring for 10 min at room temperature when the solution turned from colourless to brownish-yellow and the solution was incubated at 80–100 °C for 30 min to observe that the solution became brilliant-yellow and that the S was completely dissolved. An equal volume of water was immediately added to the reaction mixture, and the mixture solution was allowed to buff. Next, EDC/NHS was dissolved in Milli-Q water and stirred for 30 min to obtain the EDC/NHS (20 mM/20 mM) solution and the buff reaction solution was incubated with EDC/NHS solution at 40 °C for 60 min. Then, 1 mL bFGF (2000 IU) was added to the reaction solution dropwise for 12 h at 40 °C. Finally, the solution was dialyzed for 72 h to remove the free bFGF and the solution was filtered through a 0.22 μm filter membrane to obtain the Nano-S@bFGF solution.

Transmission electron microscopy (TEM) samples were prepared by dispersing the samples onto a holey carbon film on copper grids. The micrographs were obtained on a Tecnai G220 (Shimadzu, Japan) at 200 keV. Scanning electron microscopy (SEM) images of the samples were obtained by dispersing the samples on a copper table after gold spraying. The micrographs were obtained on a ZEISS Sigma 300. The micrographs were obtained on a Tecnai G220 (Shimadzu, Japan) at 200 keV. Atomic force microscopy (AFM) samples were prepared by dispersing the samples onto the mica sheets. The micrographs were obtained on a Bioscope Catalyst. Dynamic light scattering (DLS) particle size analyser (Malvern 2000, USA) samples were prepared by dispersing the samples (1 mL) onto a quartz colorimetric dish used to determine the hydrophilic diameters of the particles. Binding between bFGF and Nano-S was detected by infrared spectroscopy (IRAffinity-1S, Japan). Unless otherwise mentioned, all the measurements were performed at room temperature.

2.5. Zebrafish fin tissue regeneration model

Wild-type adult zebrafish (4–8 months old) were anesthetized in 0.1 % MS-222 (20 mL) and the half of caudal fins were amputated using a scalpel. Then, the experimental group was treated with drugs (50 mL) every other day for 8 days. Finally, zebrafish were anesthetized with 0.1 % MS-222 (20 mL), the fin regeneration length was collected by fluorescence microscopy (Mingmei Optoelectronics Technology Co. Ltd.) for analysis at different time points and the regeneration rate of caudal fin was quantified by ImageJ. All animal experiments complied with the Arrive guidelines and were carried out in accordance with the National Institutes of Health Guide for the Care and Use of Laboratory Animals.

2.6. Balb/c mice wound model and treatment

Balb/c mice (20–22 g) were provided by Guangdong Medical Laboratory Animal Center. Balb/c mice were anesthetized by intraperitoneal injection of pentobarbital sodium (100 μL). After the mice were anesthetized, a skin perforator with a diameter of 6 mm was used to construct a skin wound healing model on the backs of the mice. After the wound healing model was constructed, PBS (50 μL), Nano-S (50 μL), bFGF (50 μL) and Nano-S@bFGF (50 μL) were administered subcutaneously at the wound site every other day for 8 days. Acquired images and ImageJ were used to quantify the wound healing rate based on five different fields of

vision. Regeneration skin tissue was additionally collected from PBS, Nano-S, bFGF and Nano-S@bFGF group mice for H&E staining and the major organs (heart, liver, spleen, lung and kidney) were used for H&E staining for toxicity research. The animals were maintained in accordance with the Guide for the Care and Use of Laboratory Animals issued by the National Institutes of Health and approved by the Laboratory Animal Ethics Committee of Jinan University.

2.7. Diabetic mice wound model and treatment

8-week-old BKS db/db mice (30–35 g) were provided by Guangdong Medical Laboratory Animal Center. db/db mice were anesthetized by intraperitoneal injection of pentobarbital sodium (100 μL). After the mice were anesthetized, a skin perforator with a diameter of 6 mm was used to construct a skin wound healing model on the backs of the db/db mice mice. After the wound healing model was constructed, PBS (50 μL), Nano-S (50 μL), bFGF (50 μL) and Nano-S@bFGF (50 μL) were administered subcutaneously at the wound site every other day for 10 days. Acquired images and ImageJ were used to quantify the wound healing rate based on five different fields of vision. Regeneration skin tissue was additionally collected from the PBS and Nano-S@bFGF group mice for CD86, CD163, CD206, ARG1, iNOS1, TNF-a, Yap, *p*-FGFR and H&E staining. The animals were maintained in accordance with the Guide for the Care and Use of Laboratory Animals issued by the National Institutes of Health and approved by the Laboratory Animal Ethics Committee of Jinan University.

2.8. CCK8 assay

The digested cells were inoculated at a dilution of 2×10^3 cells/well into a 96-well plate and incubated in a 37 °C 5 % CO_2 incubator for 24 h. Then, the cells were treated with DMEM (0.5 % FBS) for 24 h for starvation and to remove the medium. Nano-S, Nano-Se, Nano-Se@S, AZD4547, Verteporfin, bFGF and Nano-S@bFGF were diluted with 0.5 % starvation medium to different concentrations, the DMEM (0.5 % FBS) as control and the same volume (100 μL) was added to each well. The cells were cultured for 48 h, and the medium was removed. Next, 100 μL/well CKK-8 solution was added for 1 h. Finally, the absorbance of each well at 450 nm was measured with a microplate analyzer.

2.9. Clonal formation assay

Cells were seeded in 6-well plates at about 500–1000 cells/well and treated with different concentrations of Nano-S, Nano-Se, Nano-Se@S, AZD4547, Verteporfin, bFGF and Nano-S@bFGF for about 2 weeks for colonies to form. The cell culture medium was discarded and then colonies were fixed. Colonies were stained with crystal violet for about 20 min and washed 3 times using distilled water. Colonies were photographed and counted.

2.10. Scratch test assay

The digested cells were inoculated at a dilution of 4×10^4 cells/well into a six-well plate, incubated in a 37 °C 5 % CO_2 incubator for 24 h to form a monolayer, and then treated with DMEM (0.5 % FBS) for 12 h for starvation. A line was then scratched on the culture using a tip (200 μL pipet) orthogonal to the mark on the plate, and the six-well plate was shaken carefully with PBS to remove floating or dead cells. Nano-S, Nano-Se, Nano-Se@S, AZD4547, Verteporfin, bFGF and Nano-S@bFGF were diluted with 0.5 % starvation medium to different concentrations, and the same volume was added to each well and cultured for 24 h. Images were acquired with a microscope, and ImageJ was used to quantify cell migration activity. The average migration rate was calculated based on five different fields of vision.

2.11. BeyoClick™ EdU assay

A total of 3×10^3 cells/mL were added to a 12-well plate, incubated in a 37 °C 5 % CO_2 incubator for 12 h, treated with DMEM (0.5 % FBS) for 24 h for starvation and medium removal. Then, the cells were treated with different concentrations of Nano-S, Nano-Se, Nano-Se@S, AZD4547, Verteporfin, bFGF and Nano-S@bFGF for 48 h. Finally, the cells were treated according to the instructions of the BeyoClick™ EdU kit, and five different fields of view were randomly selected to determine the cell proliferation rate. Proliferation rate = number of proliferating cells/total number of cells × 100 %

2.12. Evaluation of Nano-S@bFGF on the developmental toxicity of zebrafish

Wild-type juvenile zebrafish (24 hpf) were placed into 24-well plates, and each well contained 10 strips. Then, Nano-S (200 nM), bFGF (500 IU) and Nano-S@bFGF(200 nM: 500 IU) was treated every other day. The number of zebrafish that survived and hatched in each well was recorded every 24 h until for 3 days. The heartbeat of each zebrafish in each group was counted (times/min), and the zebrafish body length in each group was measured at 72 h.

2.13. Data analysis

The data are expressed as the mean ± standard deviation (SD). Data were analyzed using GraphPad Prism 8.0 software (one-way ANOVA or two-way ANOVA, (*) for $p < 0.05$, (**) for $p < 0.01$, (***) for $p < 0.001$, and (****) for $p < 0.0001$)

3. Results

3.1. The role of Se and S element accelerated in tissue regeneration

To investigate the role of Se and S during tissue regeneration, transcriptome analysis was performed (Fig. 1A). Fig. 1B shows that treatment with Nano-Se resulted in 600 differentially expressed genes (238 upregulated and 362 downregulated), while Nano-S treatment resulted in 1759 differentially expresses genes (794 upregulated and 965 downregulated). GSEA indicated that the FGFR and Hippo pathways were involved in the Nano-Se and Nano-S, respectively (Fig. 1C). In particular, Nano-Se upregulated genes within the FGFR pathway, including *fgfr1, fgfr2, fgf2,* and *fgf11*, while downregulated the Hippo pathway genes, such as *yap1, tead2, tead3*. In contrast, the expression trends of FGFR and Hippo-related genes were opposite after treated with Nano-S (Fig. 1D). These results suggested that Se and S might promote wound healing through FGFR and Hippo pathways, respectively (Fig. 1E).

To further evaluate the importance of these two pathways during tissue regeneration stimulated by Nano-Se@S, AZD4547 (FGFR inhibitor) and verteporfin (disrupting YAP-TEAD interactions) were uesd to block the FGFR and Hippo pathways. CCK8, colony formation, and EdU assays were performed in HSF cells following treatment with Nano-Se@S, AZD4547, or verteporfin. The results demonstrated that the proliferation promoted by Nano-Se@S was decreased in the Nano-Se and Nano-S groups when the Hippo (Fig. 2A–D) and FGFR (Fig. 3A–D) pathways were inactivated, respectively. Moreover, flow cytometry analysis of EdU^+ cells was conducted to quantify the proliferating cells, and consistent results were also observed when the Hippo (Fig. 2E and F) and FGFR (Fig. 3E and F) pathways were suppressed. Moreover, the effects of FGFR and Hippo signalling on Se and S in HUVECs during wound healing were evaluated by using CCK-8, colony formation, and EdU assays. Consistent results were observed in HUVECs treated with Nano-Se@S, AZD4547 (Fig. S1), or verteporfin (Fig. S2).

Zebrafish, a nonmammalian vertebrate, has become a popular disease model for research due to the high similarity of its genome with that

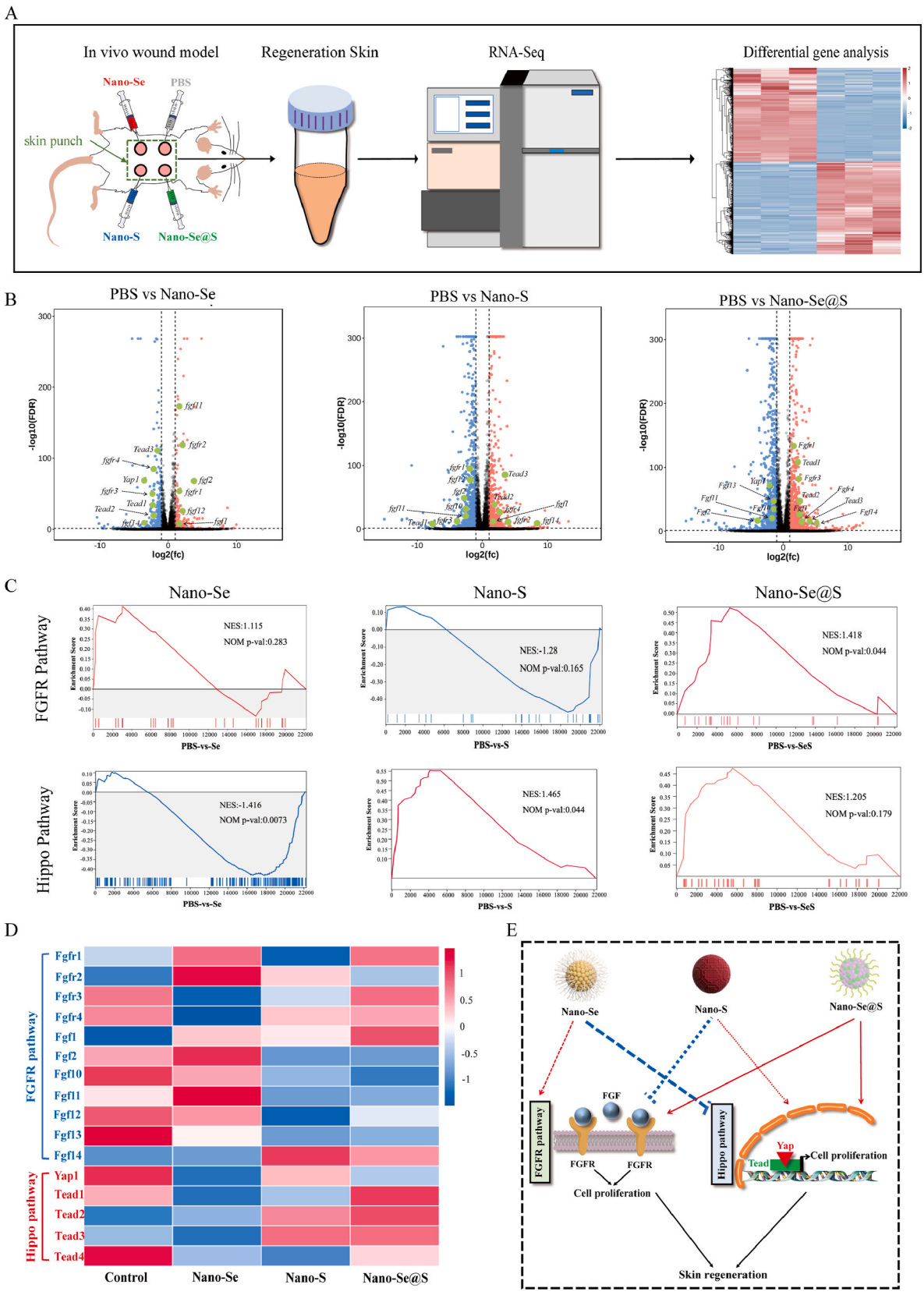

Fig. 1. RNA-Seq analysis results of Nano-Se, Nano-S and Nano-Se@S in mice. (A) Schematic illustration RNA-Seq of Nano-Se, Nano-S and Nano-Se@S. (B) Volcano maps of Nano-Se, Nano-S and Nano-Se@S significantly upregulated and downregulated genes (fold change ≥2 and P < 0.05). (C) GSEA analysis of Nano-Se, Nano-S and Nano-Se@S in FGFR and Hippo pathway. (D) Heat maps of significantly upregulated genes related to FGFR and Hippo pathway. (E) Diagram of the wound healing accelerated by Nano-Se through FGFR pathway and Nano-S through Hippo pathway.

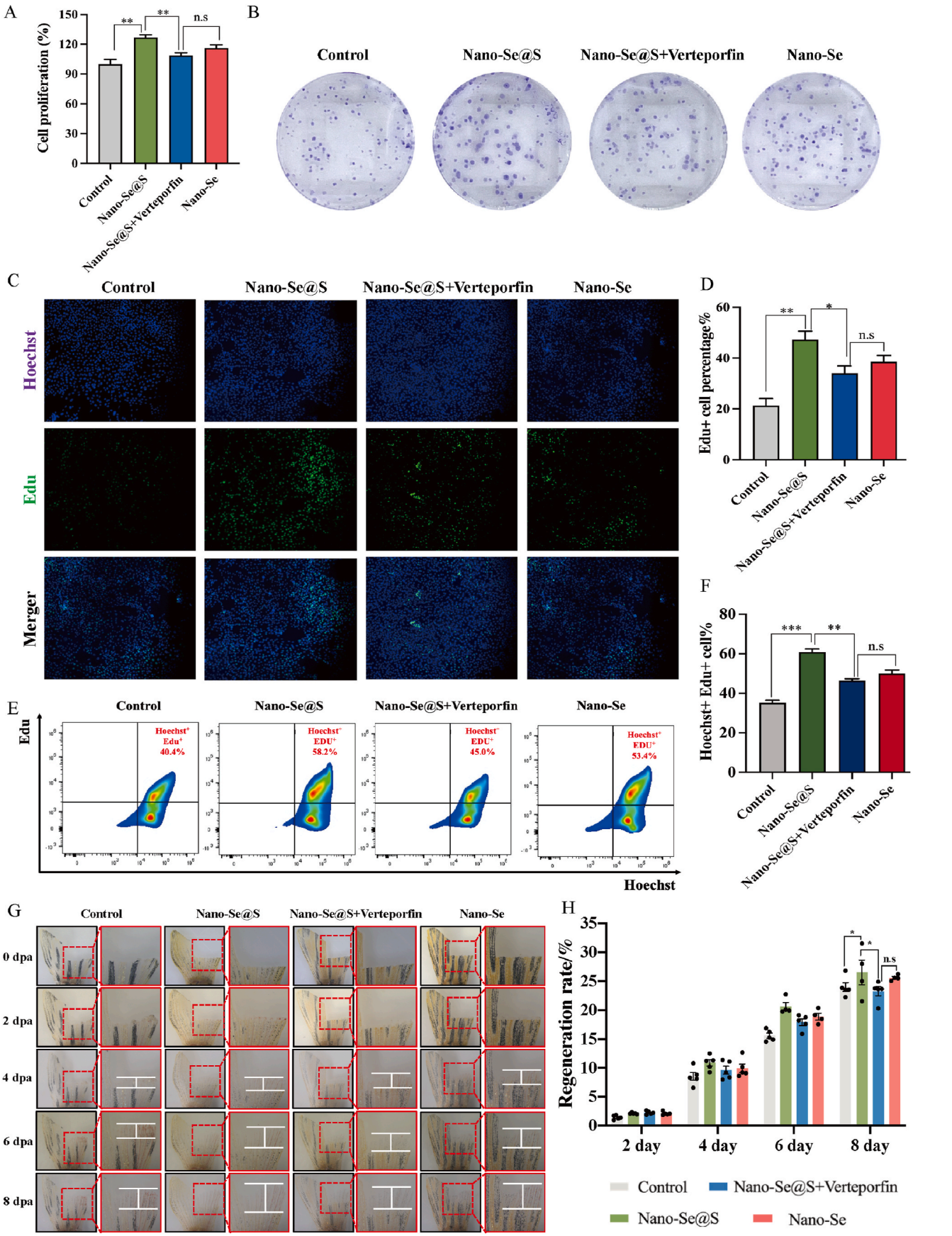

(caption on next page)

Fig. 2. Nano-S regulates Hippo signal pathway during wound healing. (A) CCK-8 assay to evaluate proliferation rate of HSF cells induced by Nano-Se@S, Nano-Se@S + Verteporfin (Hippo pathway inhibitor) and Nano-Se. (B) Clonal formation assay to evaluate proliferation rate of HSF cells induced by Nano-Se@S, Nano-Se@S + Verteporfin (Hippo pathway inhibitor) and Nano-Se. (C) Representative images of edu assay to evaluate the proliferating HSF cells induced by Nano-Se@S, Nano-Se@S + Verteporfin (Hippo pathway inhibitor) and Nano-Se. (D) Quantitative analysis of the Edu^+ cells induced by Nano-Se@S, Nano-Se@S + Verteporfin (Hippo pathway inhibitor) and Nano-Se. (E) Flow cytometry analysis of the proportion of edu^+/$hoechst^+$ cells treated with Nano-Se@S, Nano-Se@S + Verteporfin (Hippo pathway inhibitor) and Nano-Se. (F) Quantitative analysis of the edu^+/$hoechst^+$ cells induced by Nano-Se@S, Nano-Se@S + Verteporfin (Hippo pathway inhibitor) and Nano-Se. (G) Representative images of the Nano-Se@S, Nano-Se@S + Verteporfin (Hippo pathway inhibitor) and Nano-Se accelerate caudal fin regeneration. Dpa: days past amputation. (H) Regeneration rate of zebrafish caudal fin treated with Nano-Se@S, Nano-Se@S + Verteporfin (Hippo pathway inhibitor) and Nano-Se on different days. (3 independent biological repeats n = 9). (Mean values ± SD, *P < 0.05, **P < 0.01, ***P < 0.001, ****P < 0.0001).

of humans, reaching up to 80 % [22,23]. Among regenerable organs, the tail fin, which is well organized with vessels, nerves, and stromal structures and comprises skin, mesenchyme, and bone frames, has been widely used as a model to study tissue regeneration due to its repeatability, ease of manipulation, and time-savings [24,25]. Therefore, the zebrafish tail fin model was selected first to investigate the regeneration-enhancing activities in this study. As shown in Fig. 2G and H, Nano-Se@S-mediated acceleration of zebrafish tail fin regeneration activity was decreased when Hippo signalling was blocked. This regenerative activity of Nano-Se@S was also significantly reduced upon exposure to AZD4547, a pan FGFR inhibitor (Fig. 3G and H). Overall, Se enhances tissue regeneration primarily through activating the FGFR pathway, while S regulates the Hippo pathway to further strengthen this activity.

3.2. Design and characterization of the Nano-S@bFGF particles

Due to the Se toxicity *in vivo* [26], it is necessary to design nanodrugs for wound healing with clinical application prospects. According to our RNA-Seq findings, the FGFR pathway is regulated by Se during wound healing and bFGF, an FGFR activator, is widely used in clinic [27]. Several FDA-approved sulfur-related drugs have been applied to treat skin diseases. Therefore, we propose utilizing S and bFGF as units to construct nanomedicine with low toxicity and high-bioactivity for wound repair.

To obtain nanomedicines with stable morphology and high bioactivity, the ratio of S to bFGF units in nanocomposition was optimized. The dindahl effect (Fig. 4A) and DLS analyser (Fig. 4B) shown that the ratio of S and bFGF had a significant impact on the formation of nano-sized materials. TEM (Fig. 4C), scanning electron microscopy (Fig. S3) and atomic force microscopy images (Fig. 4E) showed that the ratio of S and bFGF is 1:1(200 nM: 500 IU). A typical uniformly distributed nanosphere structure with a diameter of approximately 80–120 nm was observed which is consistent with the DLS results (Fig. 4B). Conversely, bFGF concentration that are too high (1000 IU) or too low (250 IU) cannot a complete nanosphere structure. To investigate the interaction between S and bFGF, the zeta potential (Fig. 4D) and the surface roughness (Fig. 4G) were measured, and the results showed that bFGF was primarily bound to the surface of the Nano-S. Further analysis of the covalent interaction between bFGF and S was conducted via infrared spectrum analysis (Fig. 4H). Based on these findings, it was determined that the optimal combination ratio of S to bFGF for the creation of stable nanocomposites was determined to be 200 nM: 500 IU.

3.3. Nano-S@bFGF accelerated the tissue regeneration

To investigate the pro-regenerative activity of different preparation conditions Nano-S@bFGF, HSF and HUVECs were uesd. After treatment with Nano-S@bFGF for 48 h, the number of EdU^+ cells were significantly increased (Fig. 5E and Fig. S6C). By flow cytometry analysis, it was found that the highest pro-proliferative activity was observed when the ratio of S to bFGF was 1:1, with the percentage of EdU^+ cells reaching 55–60 % higher than the 15–20 % in the Ctrl group (Fig. 5G and Fig. S6D). The CCK8 (Fig. 5C and Fig. S6A) and colony formation (Fig. 5A and Fig. S6B) results were consistent with the EdU^+ results. Moreover, the migration of the cells in the Nano-S@bFGF group was assessed by a scratch test assay (Fig. 5B and Fig. S6E), and the extent of cell migration continued to increase to 58–62 % after treatment with Nano-S@bFGF (1:1) for 24 h, while the percentage of migrating cells in the Ctrl and bFGF groups decreased to 39 % and 45–50 %, respectively (Fig. 5D and Fig. S6F).

To further confirm the effect of Nano-S@bFGF on tissue regeneration *in vivo*, a zebrafish tail fin regeneration model was used to study the tissue regeneration activities of Nano-S@bFGF. As shown in Fig. 5I, tissue regeneration increased to 28.3 % after treatment with Nano-S@bFGF (1:1) for 8 days compared to 22.1 % in the control group (Fig. 5J). These results collectively indicated that the tissue regeneration-stimulated activity of Nano-S@bFGF (1:1) is conserved between zebrafish andother species.

3.4. Nano-S@bFGF accelerated the wound healing in Balb/c mice

To comparatively evaluate whether Nano-S@bFGF accelerates wound healing capacity *in vivo*, normal saline (Ctrl), Nano-S (200 nM), bFGF (500 IU) and Nano-S@bFGF (200 nM: 500 IU) were injected at a fixed point around the equirotal wounds, which is a model of the full-thickness defect in Balb/c mice (Fig. 6A). As shown in Fig. 6B and C, based on images of the wound and quantitative analysis of the wound area, the Nano-S@bFGF group showed the fastest wound healing on the 8th day, followed by the bFGF group, and the effects of Nano-S were similar to those of ctrl group. H&E staining demonstrated that the Nano-S@bFGF group exhibited the greatest recovery of the epidermal layer thickness and dermal integrity within 8 days, along with obvious hair follicle regeneration and no obvious inflammatory cell infiltration (Fig. 6D). Collectively, Nano-S@bFGF has an excellent performance in skin tissue regeneration.

3.5. Nano-S@bFGF accelerated the wound healing in db^-/db^- diabetic mice

However, refractory diabetic wound repair is a challenging problem in wound healing, and no effective drugs are available to treat this process. To evaluate the efficacy of Nano-S@bFGF in refractory wounds, db^-/db^- mice were used to construct a diabetic refractory wound model (Fig. 7A). As expected, compared with Nano-S and bFGF, Nano-S@bFGF significantly promoted wound healing on the 10th day, while the Nano-S and bFGF had no significant effect on refractory wounds (Fig. 7B and C). H&E staining revealed that the Nano-S@bFGF resulted in the greatest recovery of the skin layer structure, epidermal layer thickness and dermal integrity within 10 days (Fig. 7D). Additionally, the regulation of the inflammatory response is crucial for accelerating refractory wound repair. Immunohistochemistry (IHC) and immunofluorescence (IF) were used to detect the polarization of macrophages in the wound tissue after treatment with Nano-S@bFGF. As shown in Fig. 8A and B, compared with those in the ctrl group, the decreased in the expression of CD86 (M1 marker) and increased in the expression of CD163, ARG1, iNOS1 and TNF-α (M2 marker) were most pronounced in the Nano-S@bFGF group, suggesting that Nano-S@bFGF induces M2 polarization in the diabetic wound repair, which is conducive to the repair of diabetic refractory wounds. In addition, IF was used to detect FGFR, and the Hippo signalling pathway was activated during the Nano-S@bFGF-mediated promotion of diabetic wound repair, as shown in Fig. 8C, the protein

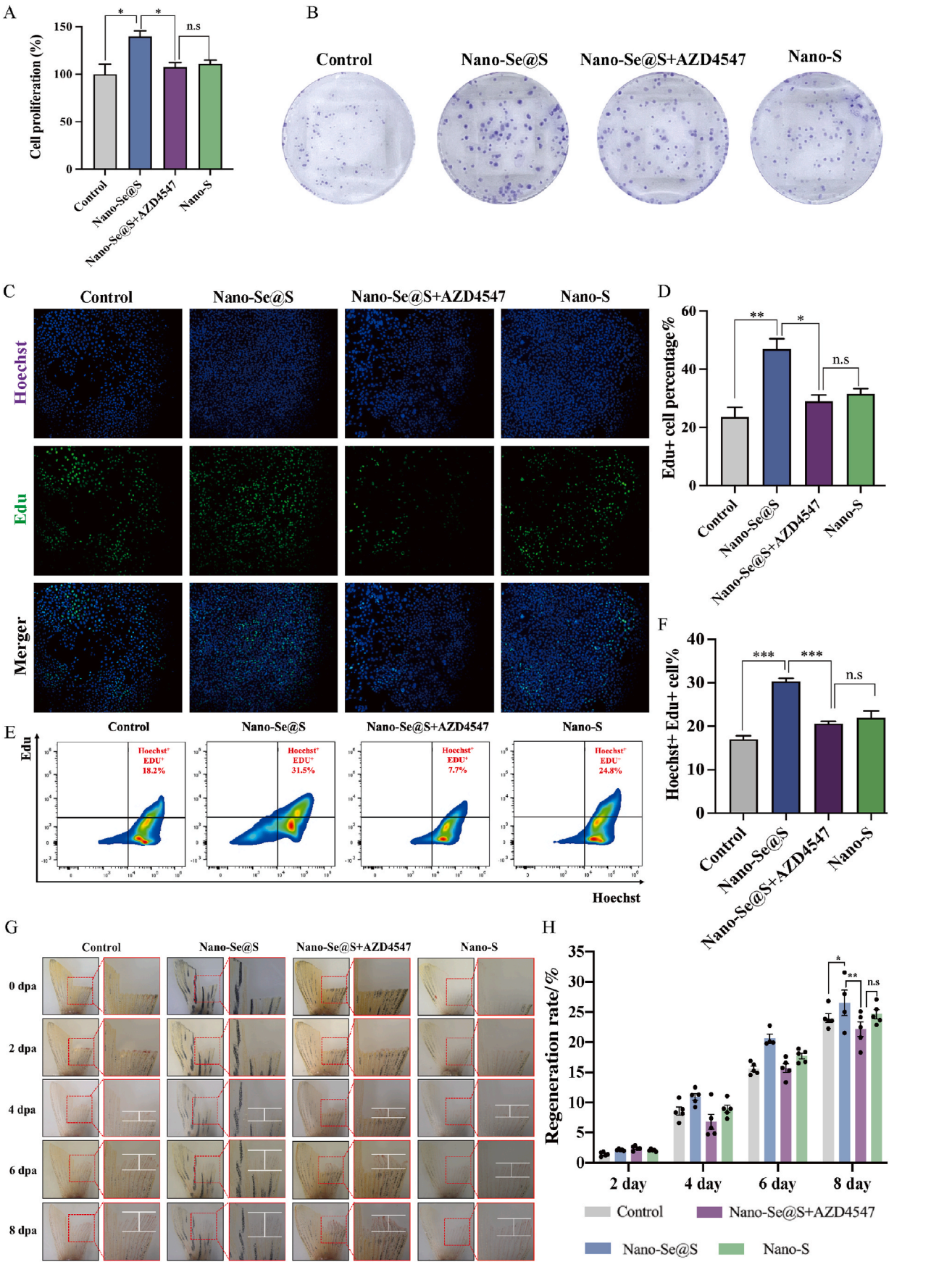

(caption on next page)

Fig. 3. Nano-Se regulates FGFR signal pathway during wound healing. (A) CCK-8 assay to evaluate proliferation rate of HSF cells induced by Nano-Se@S, Nano-Se@S + AZD4547 (FGFR pathway inhibitor) and Nano-S. (B) Clonal formation assay to evaluate proliferation rate of HSF cells induced by Nano-Se@S, Nano-Se@S + AZD4547 (FGFR pathway inhibitor) and Nano-S. (C) Representative images of edu assay to evaluate the proliferating HSF cells induced by Nano-Se@S, Nano-Se@S + AZD4547 (FGFR pathway inhibitor) and Nano-S. (D) Quantitative analysis of the Edu^+ cells induced by Nano-Se@S, Nano-Se@S + AZD4547 (FGFR pathway inhibitor) and Nano-S. (E) Flow cytometry analysis of the proportion of edu^+/$hoechst^+$ cells treated with Nano-Se@S, Nano-Se@S + AZD4547 (FGFR pathway inhibitor) and Nano-S. (F) Quantitative analysis of the edu^+/$hoechst^+$ cells induced by Nano-Se@S, Nano-Se@S + AZD4547 (FGFR pathway inhibitor) and Nano-S. (G) Representative images of the Nano-Se@S, Nano-Se@S + AZD4547 (FGFR pathway inhibitor) and Nano-S accelerate caudal fin regeneration. Dpa: days past amputation. (H) Regeneration rate of zebrafish caudal fin treated with Nano-Se@S, Nano-Se@S + AZD4547 (FGFR pathway inhibitor) and Nano-S on different days. (3 independent biological repeats n = 9). (Mean values ± SD, *P < 0.05, **P < 0.01, ***P < 0.001, ****P < 0.0001).

expression of *p*-FGFR and Yap was significantly increased after being treatment with Nano-S@bFGF. Considering the above results, the Nano-S@bFGF appears to be an excellent wound-healing agent.

3.6. The safety of Nano-S@bFGF in vivo

The safety of wound healing agents is the precondition for their use *in vivo*. To this ypothesis, the *in vivo* developmental toxicity of Nano-S@bFGF was explored in zebrafish. As expected, Nano-S@bFGF, Nano-S, and bFGF had no significant effectd on larva, as demonstrated by the images of zebrafish development after 48 h of exposure (Fig. 9A). A further index of biocompatibility was that there were no significant differences in larval survival rate (Fig. 9B), heart rate (Fig. 9C) or body length (Fig. 9D) between the Nano-S@bFGF and Ctrl groups at 48 h. The excellent biocompatibility in zebrafish prompted us to investigate its *in vivo* biosafety. To test the *in vivo* biosafety, body weight was measured in Balb/c mice bearing caudal vein injections of Nano-S@bFGF (Fig. 9E). Notably, neither caudal vein injection Nano-S@bFGF nor Nano-S caused hepatotoxicity or nephrotoxicity (Fig. 9F–I), as evidenced by alanine amiotransferase (ALT), aspartate aminotransferase (AST), UREA, and creatinine (CREA) levels. Additionally, no pathological changes were observed in the heart, liver, spleen, lung, or kidney of mice bearing caudal vein injection Nano-S@bFGF (Fig. 9J), indicating that these nanoparticles can be applied safely to organisms without causing major adverse effects. Undoubtedly, the above results demonstrate that Nano-S@bFGF nanoparticles have superior safety and biocompatibility.

4. Discussion

Wound healing, especially for chronic refractory wounds, poses a significant challenge to global health care systems and there are no effective drugs available for treating diabetic ulcers due to the hyperglycaemic, inflammatory microenvironment [28,29]. In this study, we demonstrated that Nano-S@bFGF promotes wound healing through the FGFR and Hippo signalling pathways *in vivo*. The wound healing activities of Nano-S@bFGF are conserved across nonmammalian vertebrates (zebrafish), rodents (mice), and primates (human cells). Moreover, the results demonstrated that Nano-S@bFGF promoted the healing of chronic refractory wounds in db^-/db^- mice via the induction of macrophage polarization. Our results highlight Nano-S@bFGF as a potential candidate for treating tissue regeneration-related disorders, including hyperglycaemia-related refractory wounds.

bFGF as an extracellular signalling molecule that activates FGFR signaling to accelerate wound healing in clinic, has received special attention. Our results indicated that bFGF could enhance cell viability to improve wound healing on Balb/c mice which is consistent with previous research [30–32]. Our previous studies revealed that Nano-Se promoted tissue regeneration by activating FGFR signalling [33], but the cumulative toxicity of Se greatly limits its clinical application. Hence, the use of bFGF instead of Se in wound repair to activate the FGFR pathway may be a feasible solution. Although bFGF has showed promising results in tissue regeneration, its potential as a therapeutic agent in clinic has been hampered by enzymolysis, for example,the half-life of bFGF is only 3 min in serum at 37 °C [34]. These findings were validated by our study showing that the wound repair activity of bFGF in db^-/db^- mice was significantly reduced due to the presence of bacteria and enzymes exit in the microenvironment of diabetic wounds [35,36]. Therefore, the application of auxiliary molecules is critical to the stability and bioactivity of bFGF in wound healing, especially in diabetic wounds.

Recently, biomaterials, including but not limited to peptide hydrogels [37,38], inorganic nanoparticles [39] and hydrogel dressings [40,41], has been widely used for refractory diabetic wound healing. Compared to other biomaterials, nanoparticles have unique advantages in wound healing. 1). Nanoparticles have a large specific surface area and improve the adhesion of cells associated with tissue regeneration [42]. 2). Nps, including but not limited to nanosilver, nanogold, and zinc oxide with proregenerative activity, can be modified to control the release of functional components, including polypeptides and nucleic acids [43].; 3). Nps can be loaded with different active molecules with timing control, which is beneficial for diabetes wound healing [44]; 4). The nanoparticles had excellent tissue permeability [45]. In this study, we prepared Nano-S particles loaded with bFGF, and construct Nano-S@bFGF, which was found to have an excellent effect on diabetic wound healing.

S is an important amino acid and has been widely for treating dermatological conditions, including acne, skin rash and psoriasis. Nano-S has been considered an efficient form in the biomedical field [46]. In this study, nano-S was prepared with PEG and sublimed S. Compared to the acid-catalysed precipitation of sodium thiosulfate ($Na_2S_2O_3$) and other methods [47], the PEG-modified nano-S is more stable and amenable to green-synthesis. In terms of biological activity, this study demonstrated that Nano-S showed no significant pro-regenerative activity in Balb/c and db^-/db^- mice wound healing which is consistent with our previous research [33]. Although Nano-S did not significantly promote wound healing, no tissues erosion around the wound was observed in diabetic mice. One of the probable reasons is that Nano-S has antibacterial effects [48] on diabetic wounds. In addition, we found that Nano-S could activate the Hippo pathway which regulates the shape and size during tissue development [49,50]. Our previous research revealed that the use of S as an auxiliary molecule improved the Se pro-regeneration activity and reduced the Se concentration to achieve low toxicity [19]. In addition, S has unique properties including the following: 1) several drugs containing S have been used in the clinical treatment of skin-related diseases [51], and its biosafety has been confirmed by our toxicity assay; 2) nano-S has the better transdermal efficacy due its nanostructure [52]; 3) S has antibacterial activity which is beneficial for the repair of diabetic wounds [13]. These results suggest that Nano-S may be an auxiliary molecule to improve the application of bFGF in wound healing. Therefore, we applied Nano-S and bFGF to construct Nano-S@bFGF which exhibited great tissue regeneration activity in diabetic mice at a nontoxic dose range in this study.

In this study, zebrafish fin regeneration and mice dorsal cortex injure were used as animal models for wound healing research. Although these model organisms are widely used in wound healing, there are two defects in our animal research. 1) Zebrafish with low mammalian affinity cannot demonstrate the efficacy of Nano-S@bFGF in humans. 2) Splinting plays an important role in mice wound models because the murine wounds are healed by contraction rather than re-epithelialization [53]. The acceleration of wound healing in our mice study cannot be ruled out because of skin contraction, and we will use an

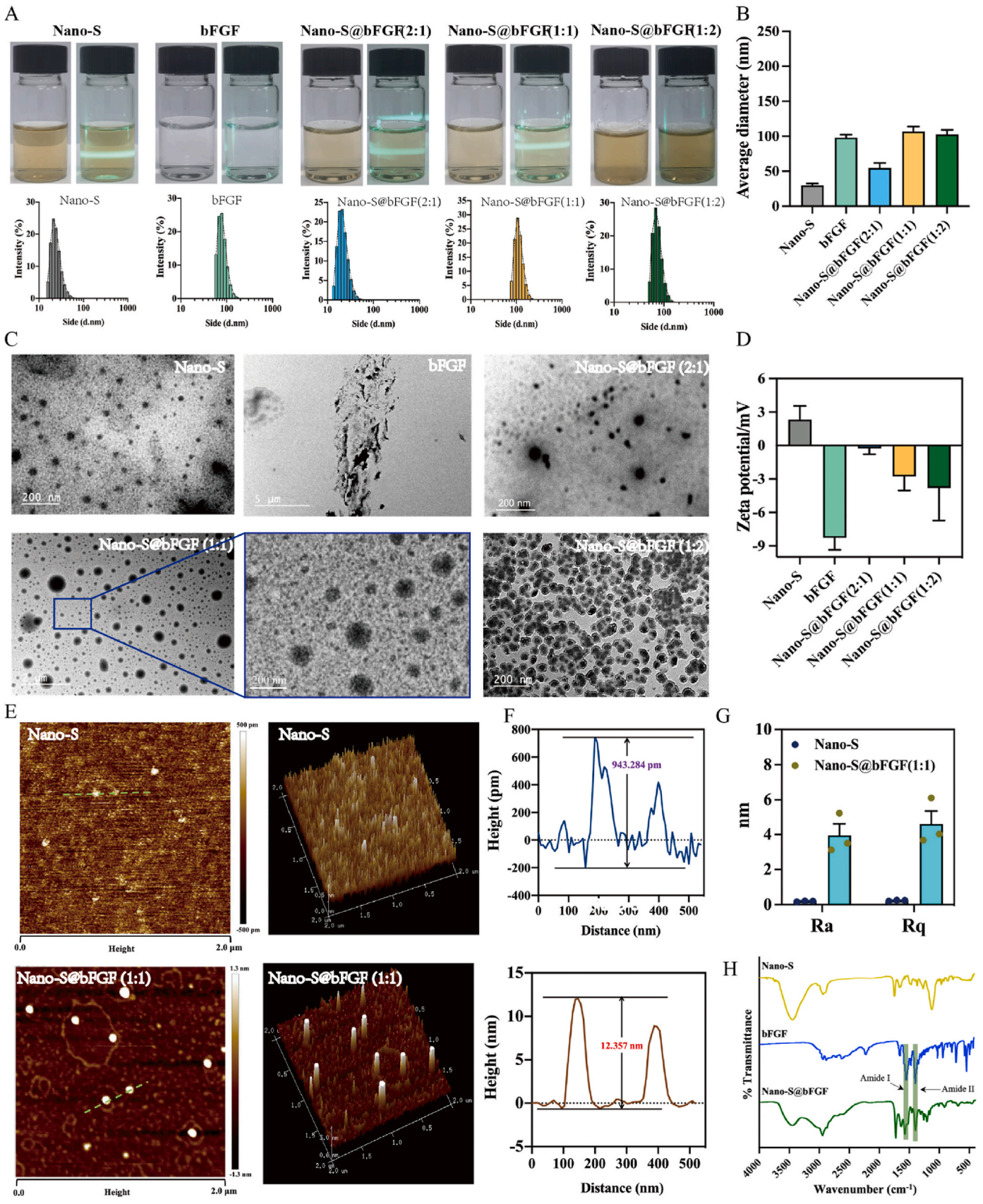

Fig. 4. Preparation and characterization of Nano-S@bFGF. (A) Dundal effect and particle size distribution (B) of the Nano-S, bFGF, Nano-S@bFGF(2:1), Nano-S@bFGF(1:1) and Nano-S@bFGF(1:2). (C) TEM image of Nano-S, bFGF, Nano-S@bFGF(2:1), Nano-S@bFGF(1:1) and Nano-S@bFGF(1:2). (D) Zeta potential analysis of Nano-S, bFGF, Nano-S@bFGF(2:1), Nano-S@bFGF(1:1) and Nano-S@bFGF(1:2). (E) AFM image, (F) particle size and (G) particle surface roughness data analysis of Nano-S and Nano-S@bFGF(1:1). (H) Infrared spectrometer analysis of Nano-S, bFGF, Nano-S@bFGF(1:1).

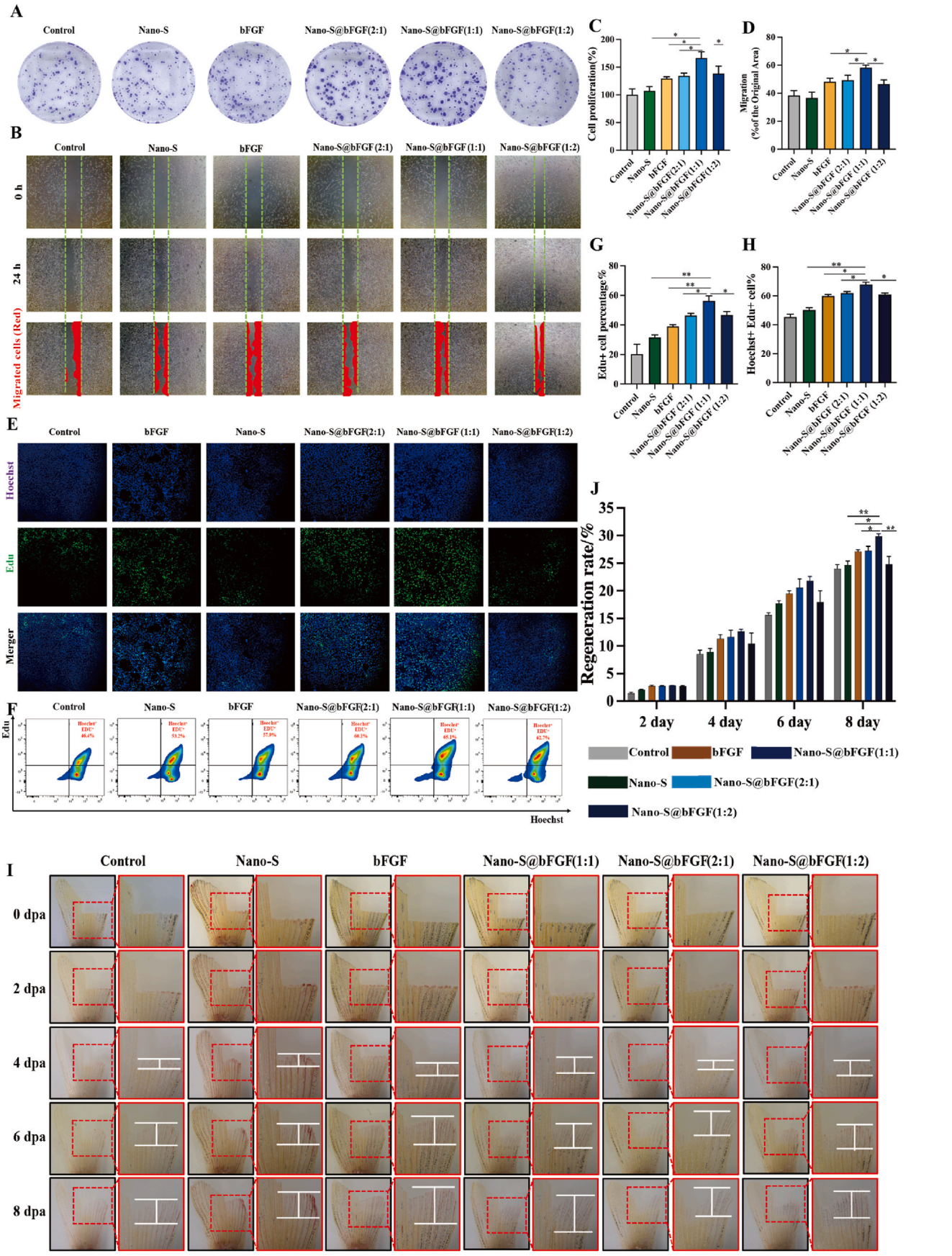

(caption on next page)

Fig. 5. Nano-S@bFGF promotes tissue regeneration in vitro and zebrafish fin regeneration. (A) Clonal formation assay to evaluate proliferation rate of HSF cells induced by Nano-S, bFGF, Nano-S@bFGF(2:1), Nano-S@bFGF(1:1) and Nano-S@bFGF(1:2). (B) Representative images of scratch assay to evaluate the migration of HSF cells induced by Nano-S, bFGF, Nano-S@bFGF(2:1), Nano-S@bFGF(1:1) and Nano-S@bFGF(1:2). (C) CCK-8 assay to evaluate proliferation rate of HSF cells induced by Nano-S, bFGF, Nano-S@bFGF(2:1), Nano-S@bFGF(1:1) and Nano-S@bFGF(1:2). (D) Migration rate of HSF cells induced by Nano-S, bFGF, Nano-S@bFGF(2:1), Nano-S@bFGF(1:1) and Nano-S@bFGF(1:2) (E) Representative images of edu assay to evaluate the proliferating HSF cells induced by Nano-S, bFGF, Nano-S@bFGF(2:1), Nano-S@bFGF(1:1) and Nano-S@bFGF(1:2). (F) Flow cytometry analysis of the proportion of edu^{+}/$hoechst^{+}$ cells treated with Nano-S, bFGF, Nano-S@bFGF(2:1), Nano-S@bFGF(1:1) and Nano-S@bFGF(1:2). (G) Quantitative analysis of the Edu^{+} cells induced by Nano-S, bFGF, Nano-S@bFGF(2:1), Nano-S@bFGF(1:1) and Nano-S@bFGF(1:2). (H) Quantitative analysis of the edu^{+}/$hoechst^{+}$ cells induced by Nano-S, bFGF, Nano-S@bFGF(2:1), Nano-S@bFGF(1:1) and Nano-S@bFGF(1:2). (I) Representative images of the Nano-S, bFGF, Nano-S@bFGF(2:1), Nano-S@bFGF(1:1) and Nano-S@bFGF(1:2) accelerate caudal fin regeneration. Dpa: days past amputation. (J) Regeneration rate of zebrafish caudal fin treated with Nano-S, bFGF, Nano-S@bFGF(2:1), Nano-S@bFGF(1:1) and Nano-S@bFGF(1:2) on different days. (3 independent biological repeats n = 9). (Mean values ± SD, *P < 0.05, **P < 0.01, ***P < 0.001, ****P < 0.0001).

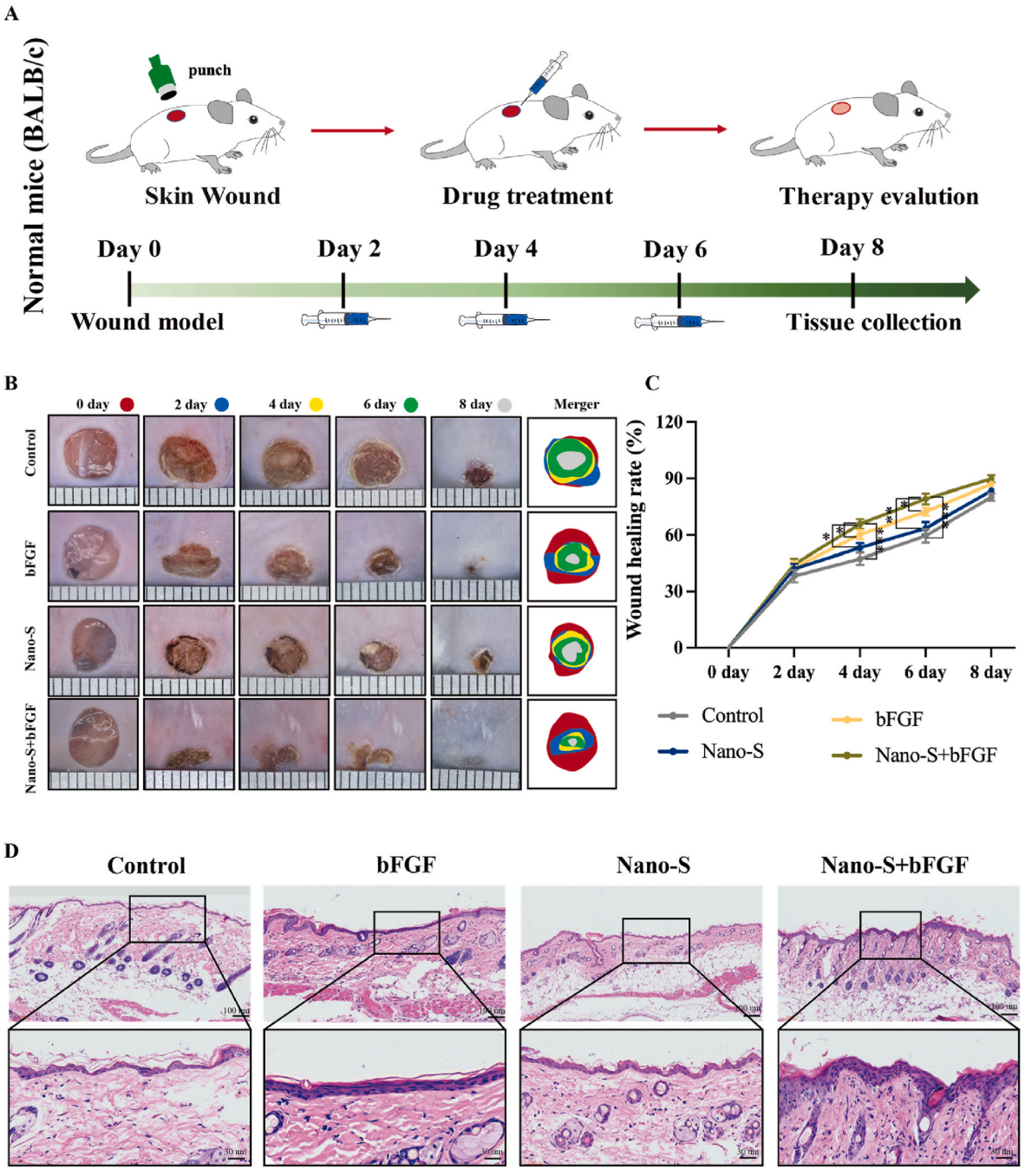

Fig. 6. Nano-S@bFGF promotes wound healing in Balb/c mice. (A) The schematic diagram for the *in vivo* treatment evaluation procedure. (B) The photographs of skin wound images treated with different concentrations of Nano-S (200 nM), bFGF (500IU), Nano-S@bFGF(200 nM:500 IU). (C) Closed area ratio of skin wounds. (D) Histological graphs of skin tissue by H&E staining. (n = 6, Mean values ± SD, *P < 0.05, **P < 0.01, ***P < 0.001, ****P < 0.0001).

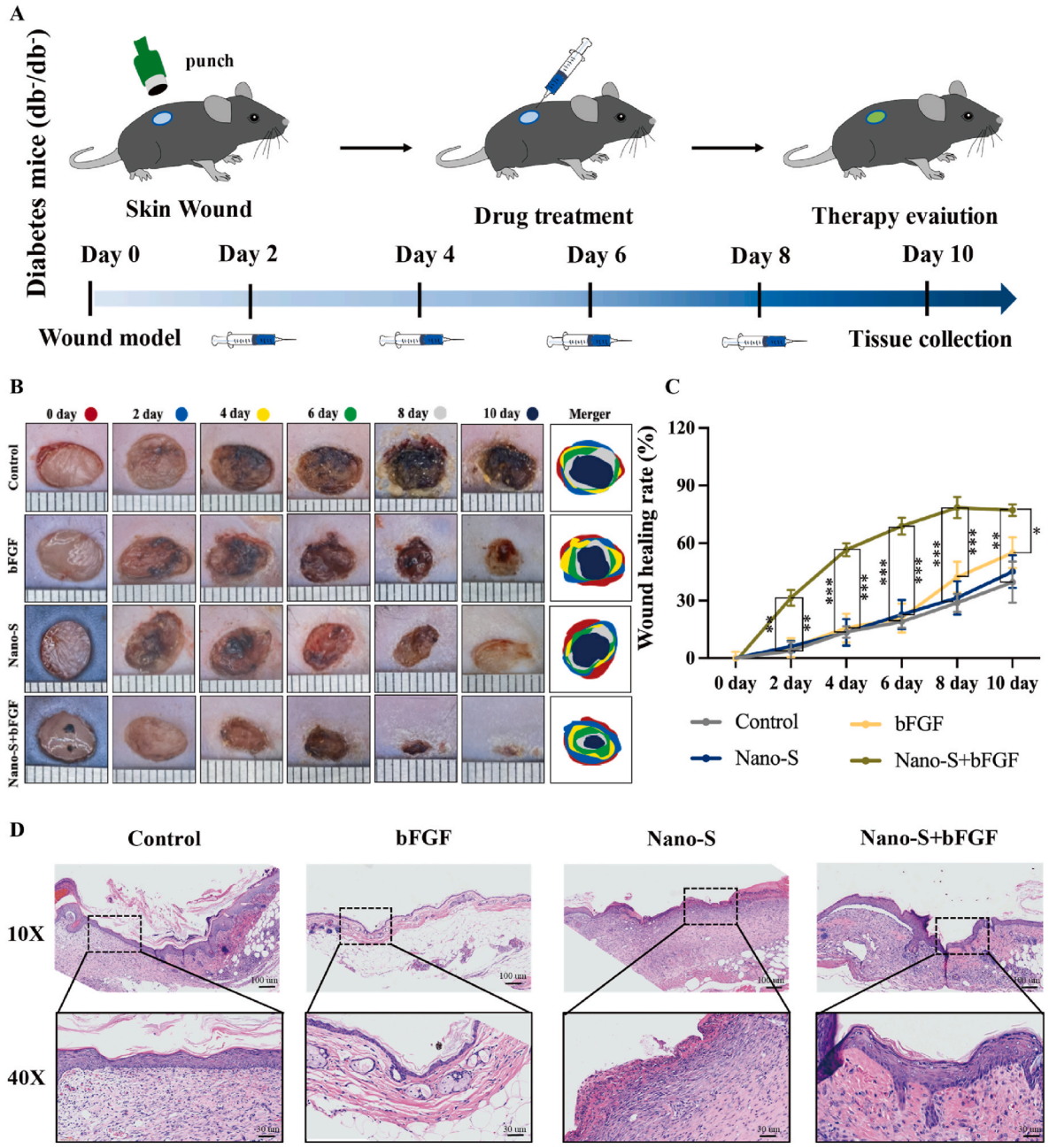

Fig. 7. Nano-S@bFGF promotes wound healing in db$^-$/db$^-$ mice. (A) The schematic diagram for the *in vivo* treatment evaluation procedure. (B) The photographs of skin wound images treated with different concentrations of Nano-S (200 nM), bFGF (500IU), Nano-S@bFGF (200 nM:500 IU). (C) Closed area ratio of skin wounds. (D) Histological graphs of skin tissue by H&E staining. (n = 6, Mean values ± SD, *P < 0.05, **P < 0.01, ***P < 0.001, ****P < 0.0001).

excisional wound splinting mice model in future studies.

Tissue regeneration is a complex process involving multiple cell types and various signalling pathways. The signalling pathways involved in tissue regeneration mainly include FGF [54], WNT [55], Hippo [56], Notch [57], Hedgehog [58], and VEGF [59]. The cell types involved in regeneration depend on the type of regenerating tissue. In this study, we found that FGFR and Hippo signalling were involved in and crucial for Nano-S@bFGF-induced wound healing. The importance of these two signalling pathways has been stressed in zebrafish [60,61] and mouse studies [62,63]. Thus, the results of our study are consistent with those of previous investigations. In addition to the FGFR and Hippo signalling pathways, inflammatory regulation also plays an important role in refractory diabetic wounds [64]. During wound healing, M1 macrophages predominate from day one to day three to prevent the infection but transits to M2 macrophages to accelerate the wound healing [65]. However, in diabetic wounds, macrophages usually remain at the M1 stage, leading to the poor angiogenesis and collagen deposition [66]. Therefore, the induction of M1 to M2 repolarization is one of the key treatments for refractory diabetic wounds. Our skin histological results of diabetic mice showed that Nano-S@bFGF can induce M2 polarization, induce wound healing from the inflammatory stage to the proliferative stage and complete refractory wound repair.

Overall, we highlighted Nano-S@bFGF as an accelerator for tissue regeneration under both physiological and pathological conditions at its nontoxic doses. Mechanistically, Nano-S@bFGF triggered FGFR and Hippo signalling-dependent tissue regeneration and induced M2 polarization *in vivo*, which is one of the classical mechanisms involved in diabetic wound healing. Our findings support the regeneration-promoting activity of Nano-S@bFGF, especially in diabetic patients.

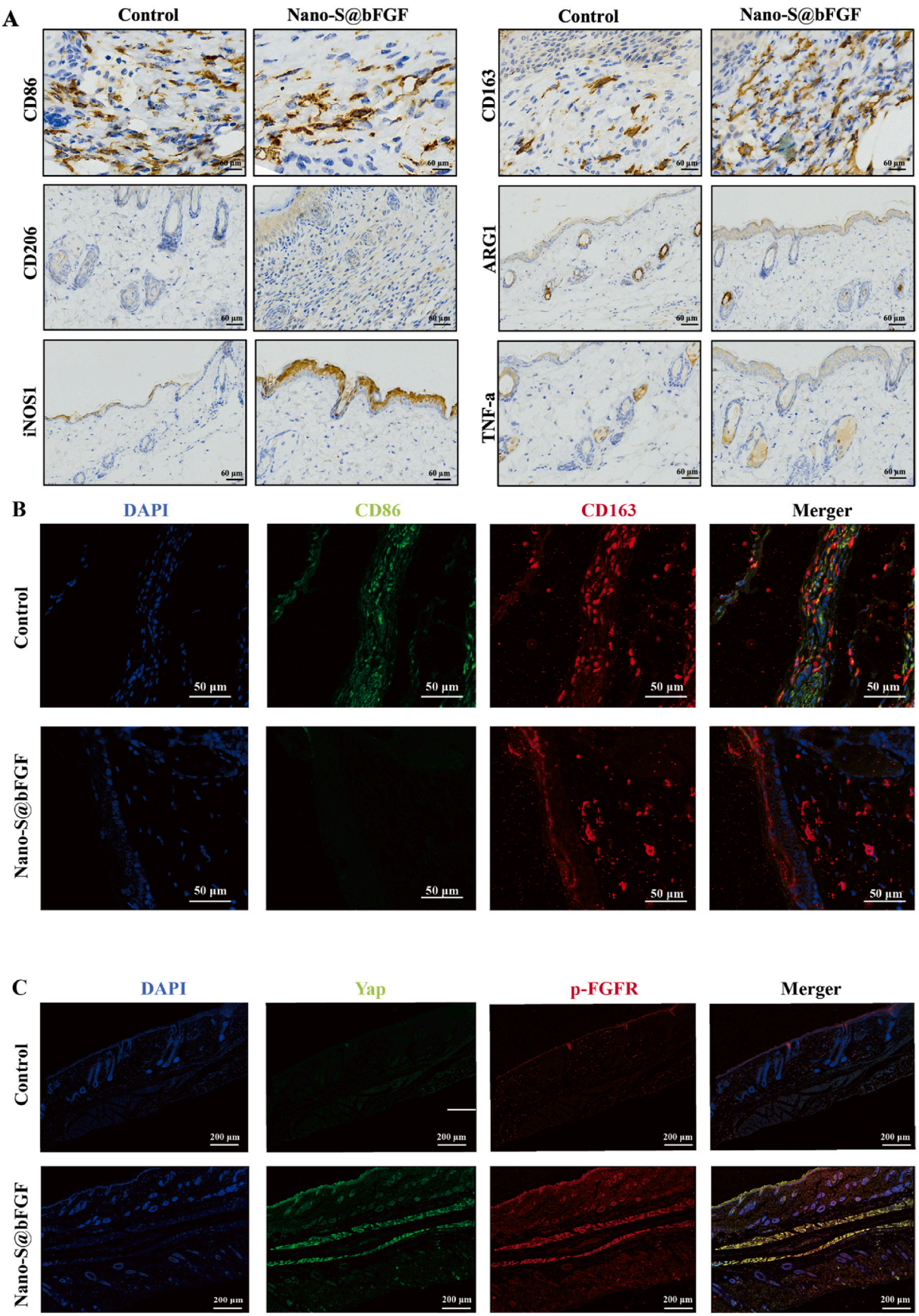

Fig. 8. Nano-S@bFGF promote macrophages M2 polarization and co-activate FGFR/Hippo pathway in diabetic wounds. (A) Immunohistochemistry of CD86 (M1 marker) and CD163, CD206, iNOS1, AGR1 and TNF-a (M2 marker) of the wound tissue (scale bar: 60 μm). (B) Immunofluorescence of CD86 and CD163 of the wound tissue (scale bar: 50 μm). (C) Immunofluorescence of Yap and *p*-FGFR of the wound tissue (scale bar: 200 μm).

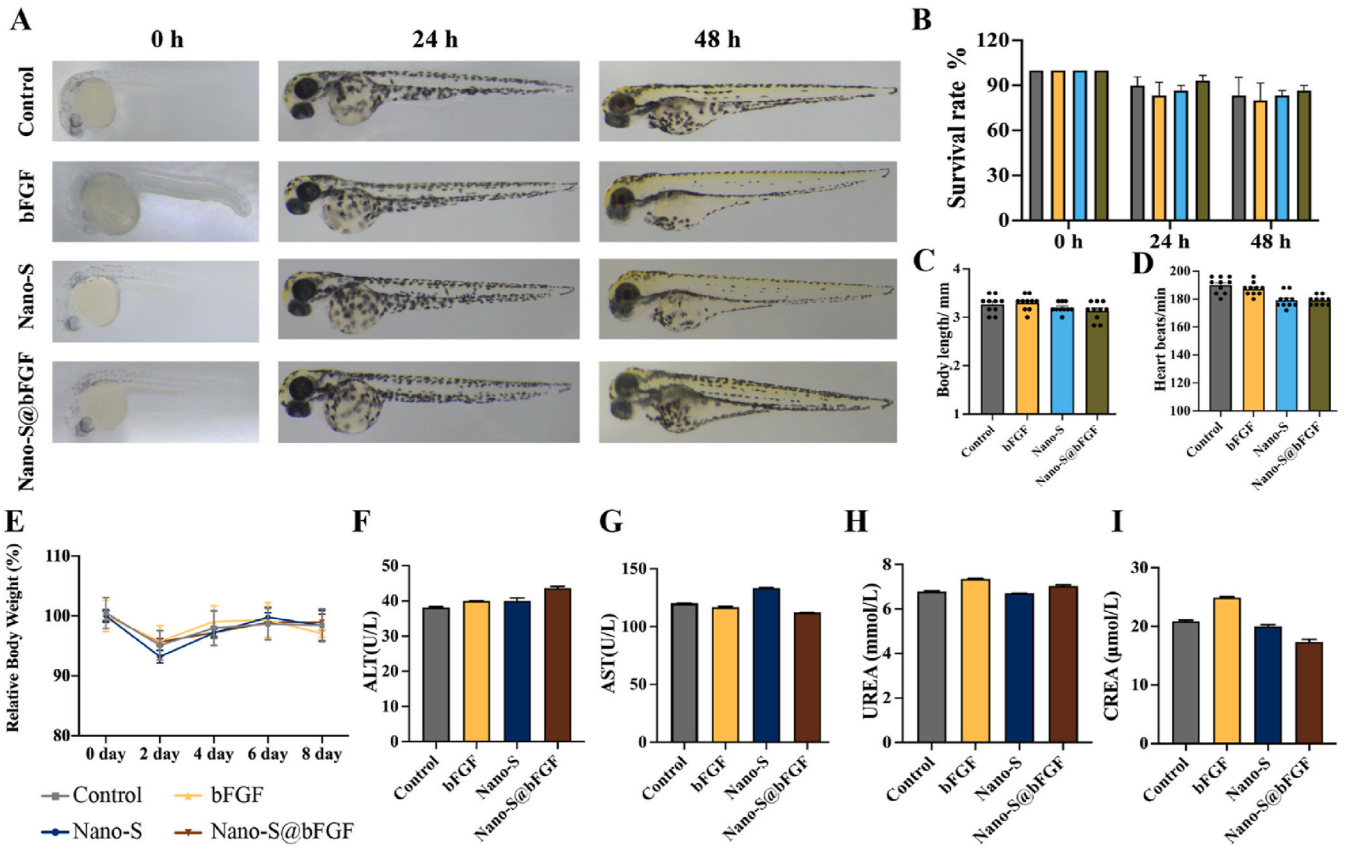

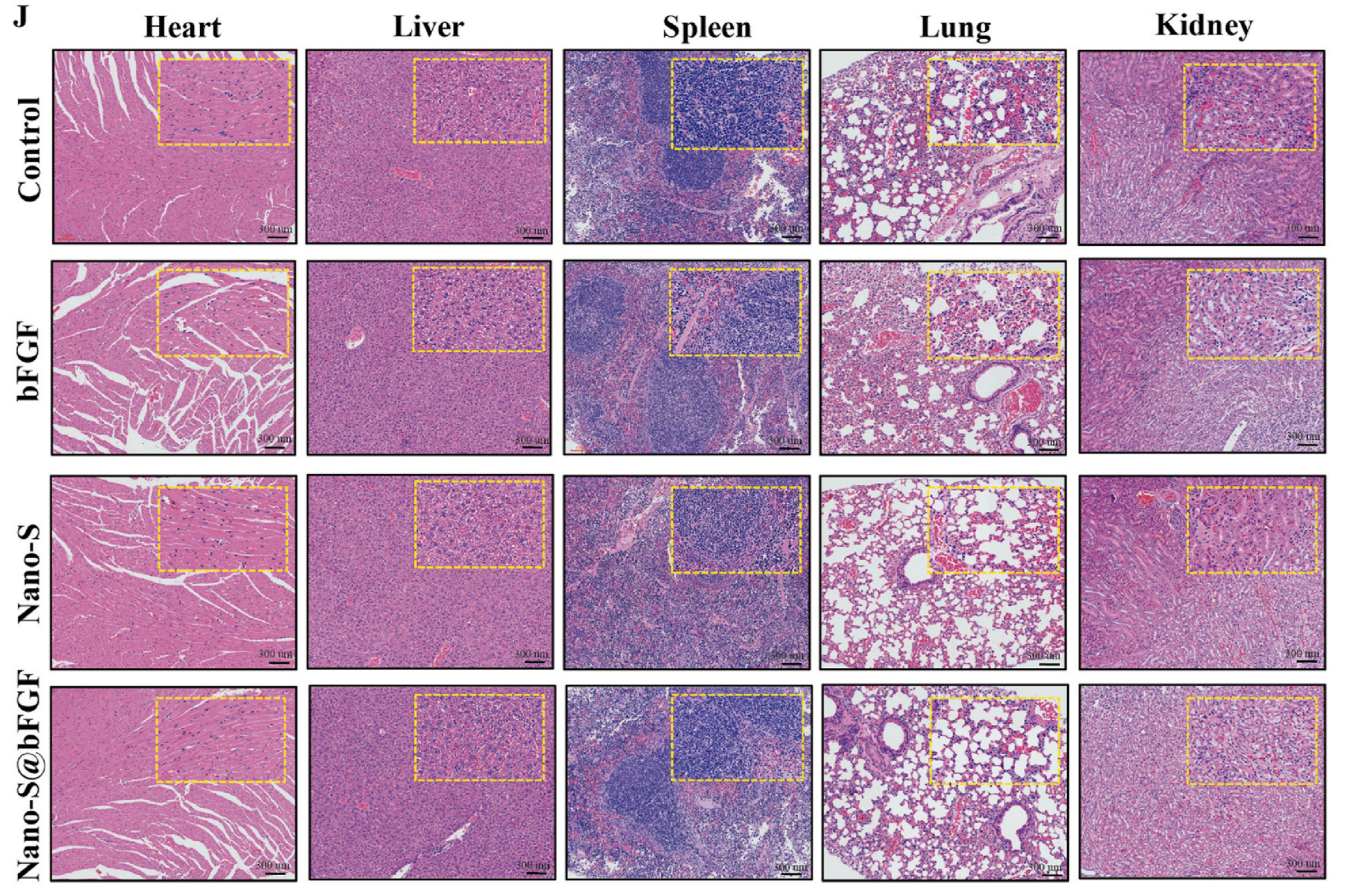

(caption on next page)

Fig. 9. Toxicity evaluation of Nano-S (200 nM), bFGF (500 IU), Nano-S@bFGF (200 nM:500 IU) in zebrafish and Balb/c mice. (A) Representative images of developmental toxicity in zebrafish treated with Nano-S (200 nM), bFGF (500 IU), Nano-S@bFGF (200 nM:500 IU). (B) Toxicity of Nano-S (200 nM), bFGF (500 IU), Nano-S@bFGF (200 nM:500 IU) was evaluated by survival rate (n = 10); (C) Toxicity of Nano-S (200 nM), bFGF (500 IU), Nano-S@bFGF (200 nM:500 IU) was evaluated by body length in 48 h (n = 10). (D) Toxicity of Nano-S (200 nM), bFGF (500 IU), Nano-S@bFGF (200 nM:500 IU) was evaluated by heart beats/1 min in 48 h (n = 10). (E) Body weight of mice treated with Nano-S (200 nM), bFGF (500 IU), Nano-S@bFGF (200 nM:500 IU). The change profiles of ALT(F), AST(G), UREA (H) and CREA(I) treated with Nano-S (200 nM), bFGF (500 IU), Nano-S@bFGF (200 nM:500 IU). (J) H&E staining of major organs (heart, liver, spleen, lung and kidney) showing the biosafety of Nano-S (200 nM), bFGF (500 IU), Nano-S@bFGF (200 nM:500 IU), Scale bar is 300 μm. Yellow box: 5 times magnification image (n = 6).

5. Conclusion

In summary, we illustrated PEG modification methods for hydrosoluble Nano-S@bFGF synthesis and revealed that Nano-S@bFGF facilitates great wound healing bioactivity with reduced toxicity using mice, zebrafish, and human cells. Mechanistically, Nano-S@bFGF not only promoted normal tissue regeneration through the FGFR and Hippo signalling pathways but also promoted skin epair in diabetic mice by inducing the repolarization of macrophages around the wound. This work demonstrated the possibility of applying Nano-S@bFGF for skin regeneration, especially for the refractory diabetic wounds. This research not only broadens the application scenarios of S and bFGF; but also provides a new treatment approach for the regeneration of clinically refractory diabetic wound. In future work, we will conduct in-depth research on the appropriate pharmaceutical formulations to provide a foundation for human clinical therapy.

Availability of data and materials

The data that support the findings of this study are available from the corresponding author upon reasonable request.

Ethics approval and consent to participate

All animal experiments were approved by the research ethics committee of Jinan University.

Consent for publication

All authors gave their consent for publication.

CRediT authorship contribution statement

Jieqiong Cao: Writing – original draft, Methodology, Formal analysis, Conceptualization. **Zijian Su:** Writing – review & editing, Methodology, Investigation, Formal analysis. **Yibo Zhang:** Writing – review & editing, Funding acquisition, Formal analysis, Conceptualization. **Zhiqi Chen:** Methodology, Formal analysis. **Jingsheng Li:** Methodology. **Yulin Cai:** Methodology. **Yiming Chang:** Methodology. **Minghua Lei:** Methodology. **Qianyi He:** Methodology. **Weicai Li:** Methodology. **Xuan Liao:** Funding acquisition. **Shuixing Zhang:** Project administration, Funding acquisition. **An Hong:** Supervision, Project administration, Funding acquisition, Conceptualization. **Xiaojia Chen:** Writing – review & editing, Funding acquisition, Conceptualization.

Declaration of competing interest

The authors declare the following financial interests/personal relationships which may be considered as potential competing interests: Xiaojia Chen reports financial support was provided by Jinan University. Xiaojia Chen reports a relationship with Jinan University that includes: non-financial support. Xiaojia Chen, An Hong, Jieqiong Cao, Yibo Zhang, Zijian Su has patent pending to Nano-S@bFGF. The remaining authors declare no potential conflict of interests. If there are other authors, they declare that they have no known competing financial interests or personal relationships that could have appeared to influence the work reported in this paper.

Data availability

No data was used for the research described in the article.

Acknowledgments

This study was supported by grants from the National Natural Science Foundation of China (No. 82273833, No. 82173729 and No. 82102345), Key R&D projects in Guangdong Province (No. 2022B111070007), Guangzhou Science and Technology Project (No. 2021221007), Guangdong Basic and Applied Basic Research Foundation (No. 2024A1515030168).

Appendix A. Supplementary data

Supplementary data to this article can be found online at https://doi.org/10.1016/j.mtbio.2024.101104.

References

[1] E.M. Tottoli, R. Dorati, I. Genta, E. Chiesa, S. Pisani, B. Conti, Skin wound healing process and new emerging technologies for skin wound care and regeneration, Pharmaceutics 12 (8) (2020), https://doi.org/10.3390/pharmaceutics12080735.
[2] M. Olsson, K. Jarbrink, U. Divakar, R. Bajpai, Z. Upton, A. Schmidtchen, et al., The humanistic and economic burden of chronic wounds: a systematic review, Wound Repair Regen 27 (1) (2019) 114–125, https://doi.org/10.1111/wrr.12683.
[3] J.A. Goldman, K.D. Poss, Gene regulatory programmes of tissue regeneration, Nat Rev Genet 21 (9) (2020) 511–525, https://doi.org/10.1038/s41576-020-0239-7.
[4] B. Zhao, K. Tumaneng, K.L. Guan, The Hippo pathway in organ size control, tissue regeneration and stem cell self-renewal, Nat Cell Biol 13 (8) (2011) 877–883, https://doi.org/10.1038/ncb2303.
[5] Y. Xie, N. Su, J. Yang, Q. Tan, S. Huang, M. Jin, et al., FGF/FGFR signaling in health and disease, Signal Transduct Target Ther 5 (1) (2020) 181, https://doi.org/10.1038/s41392-020-00222-7.
[6] X. Wu, W. He, X. Mu, Y. Liu, J. Deng, Y. Liu, et al., Macrophage polarization in diabetic wound healing, Burns Trauma 10 (2022) tkac051, https://doi.org/10.1093/burnst/tkac051.
[7] D. Chouhan, B.B. Mandal, Silk biomaterials in wound healing and skin regeneration therapeutics: from bench to bedside, Acta Biomater 103 (2020) 24–51, https://doi.org/10.1016/j.actbio.2019.11.050.
[8] H. Xiao, X. Chen, X. Liu, G. Wen, Y. Yu, Recent advances in decellularized biomaterials for wound healing, Mater Today Bio 19 (2023) 100589, https://doi.org/10.1016/j.mtbio.2023.100589.
[9] Y.R. Li, Q. Meng, S.J. Chen, P.X. Ling, M.A. Kuss, B. Duan, et al., Advances, challenges, and prospects for surgical suture materials, Acta Biomaterialia 168 (2023) 78–112, https://doi.org/10.1016/j.actbio.2023.07.041.
[10] L. Qiao, Y. Liang, J. Chen, Y. Huang, S.A. Alsareii, A.M. Alamri, et al., Antibacterial conductive self-healing hydrogel wound dressing with dual dynamic bonds promotes infected wound healing, Bioact Mater 30 (2023) 129–141, https://doi.org/10.1016/j.bioactmat.2023.07.015.
[11] P. Cheng, X.D. Xie, L.C. Hu, W. Zhou, B.B. Mi, Y. Xiong, et al., Hypoxia endothelial cells-derived exosomes facilitate diabetic wound healing through improving endothelial cell function and promoting M2 macrophages polarization, Bioactive Materials 33 (2024) 157–173, https://doi.org/10.1016/j.bioactmat.2023.10.020.
[12] H. Fan, Q. Bai, Y. Yang, X. Shi, G. Du, J. Yan, et al., The key roles of reactive oxygen species in microglial inflammatory activation: regulation by endogenous antioxidant system and exogenous sulfur-containing compounds, Eur J Pharmacol 956 (2023) 175966, https://doi.org/10.1016/j.ejphar.2023.175966.
[13] R.A. Dop, D.R. Neill, T. Hasell, Sulfur-polymer nanoparticles: preparation and antibacterial activity, ACS Appl Mater Interfaces 15 (17) (2023) 20822–20832, https://doi.org/10.1021/acsami.3c03826.
[14] L. Jaiswal, S. Shankar, J.W. Rhim, Carrageenan-based functional hydrogel film reinforced with sulfur nanoparticles and grapefruit seed extract for wound healing application, Carbohydr Polym 224 (2019) 115191, https://doi.org/10.1016/j.carbpol.2019.115191.
[15] Y. Cao, A. Bairam, M.C. Liu, J. Uetrecht, Potential involvement of sulfotransferase in the mechanism of lamotrigine-induced skin rash, Chem Res Toxicol 36 (11) (2023) 1711–1716, https://doi.org/10.1021/acs.chemrestox.3c00187.

[16] Á. Kulisch, Z. Mándó, E. Sándor, Z. Lengyel, A. Illés, J. Kósa, et al., Evaluation of the effects of Lake Hévíz sulfur thermal water on skin microbiome in plaque psoriasis: an open label, pilot study 67 (4) (2023) 661–673.
[17] P.F. Xu, Z.H. Liu, Y.H. Duan, Q. Sun, D. Wang, X.F. Zeng, et al., Microfluidic controllable synthesis of monodispersed sulfur nanoparticles with enhanced antibacterial activities, Chemical Engineering Journal 398 (2020), https://doi.org/10.1016/j.cej.2020.125293.
[18] Y.A. Liu, Y.C. Gong, W.J. Xie, A.L. Huang, X.Y. Yuan, H. Zhou, et al., Microbubbles in combination with focused ultrasound for the delivery of quercetin-modified sulfur nanoparticles through the blood brain barrier into the brain parenchyma and relief of endoplasmic reticulum stress to treat Alzheimer's disease, Nanoscale 12 (11) (2020) 6498–6511, https://doi.org/10.1039/c9nr09713a.
[19] J.Q. Cao, Y.B. Zhang, Y.Q. Yang, J.Y. Xie, Z.J. Su, F. Li, et al., Turning gray selenium and sublimed sulfur into a nanocomposite to accelerate tissue regeneration by isothermal recrystallization, Journal of Nanobiotechnology 21 (1) (2023), https://doi.org/10.1186/s12951-023-01796-4.
[20] M.P. Rayman, Selenium intake, status, and health: a complex relationship, Hormones (Athens) 19 (1) (2020) 9–14, https://doi.org/10.1007/s42000-019-00125-5.
[21] I. Zwolak, The role of selenium in arsenic and cadmium toxicity: an updated review of scientific literature, Biol Trace Elem Res 193 (1) (2020) 44–63, https://doi.org/10.1007/s12011-019-01691-w.
[22] E.E. Patton, L.I. Zon, D.M. Langenau, Zebrafish disease models in drug discovery: from preclinical modelling to clinical trials, Nat Rev Drug Discov 20 (8) (2021) 611–628, https://doi.org/10.1038/s41573-021-00210-8.
[23] T.Y. Choi, T.I. Choi, Y.R. Lee, S.K. Choe, C.H. Kim, Zebrafish as an animal model for biomedical research, Experimental and Molecular Medicine 53 (3) (2021) 310–317, https://doi.org/10.1038/s12276-021-00571-5.
[24] S. Pang, Y. Gao, F. Wang, Y. Wang, M. Cao, W. Zhang, et al., Toxicity of silver nanoparticles on wound healing: a case study of zebrafish fin regeneration model, Sci Total Environ 717 (2020) 137178, https://doi.org/10.1016/j.scitotenv.2020.137178.
[25] T.A. Petrie, N.S. Strand, C.T. Yang, J.S. Rabinowitz, R.T. Moon, Macrophages modulate adult zebrafish tail fin regeneration, Development 141 (13) (2014) 2581–2591, https://doi.org/10.1242/dev.098459.
[26] B.R. Cardoso, L. Lago, A.L. Dordevic, E.A. Kapp, A.M. Raines, R.A. Sunde, et al., Differential protein expression due to Se deficiency and Se toxicity in rat liver, Journal of Nutritional Biochemistry 98 (2021), https://doi.org/10.1016/j.jnutbio.2021.108831.
[27] L. Benington, G. Rajan, C. Locher, L.Y. Lim, Fibroblast growth factor 2-A review of stabilisation approaches for clinical applications, Pharmaceutics 12 (6) (2020), https://doi.org/10.3390/pharmaceutics12060508.
[28] P. Ansari, S. Akther, J.T. Khan, S.S. Islam, M.S.R. Masud, A. Rahman, et al., Hyperglycaemia-linked diabetic foot complications and their management using conventional and alternative therapies, Applied Sciences-Basel 12 (22) (2022), https://doi.org/10.3390/app122211777.
[29] Y. Guan, H. Niu, Z. Liu, Y. Dang, J. Shen, M. Zayed, et al., Sustained oxygenation accelerates diabetic wound healing by promoting epithelialization and angiogenesis and decreasing inflammation, Sci Adv 7 (35) (2021), https://doi.org/10.1126/sciadv.abj0153.
[30] A. Chen, W. Huang, L. Wu, Y. An, T. Xuan, H. He, et al., Bioactive ECM mimic hyaluronic acid dressing via sustained releasing of bFGF for enhancing skin wound healing, ACS Appl Bio Mater 3 (5) (2020) 3039–3048, https://doi.org/10.1021/acsabm.0c00096.
[31] Y. Hao, W. Zhao, H. Zhang, W. Zheng, Q. Zhou, Carboxymethyl chitosan-based hydrogels containing fibroblast growth factors for triggering diabetic wound healing, Carbohydr Polym 287 (2022) 119336, https://doi.org/10.1016/j.carbpol.2022.119336.
[32] J. Xu, K.N. Wang, Y.Y. Li, Y. Li, B.X. Li, H.Q. Luo, et al., Injectable Host-Guest supramolecular hydrogel Co-Delivers hydrophobic and hydrophilic agents for enhanced wound healing, Chemical Engineering Journal 454 (2023), https://doi.org/10.1016/j.cej.2022.140027.
[33] J.Q. Cao, Y.B. Zhang, P.G. Zhang, Z.L. Zhang, B.H. Zhang, Y.X. Feng, et al., Turning gray selenium into a nanoaccelerator of tissue regeneration by PEG modification, Bioactive Materials 15 (2022) 131–144, https://doi.org/10.1016/j.bioactmat.2021.12.026.
[34] P. Arunkumar, J.A. Dougherty, J. Weist, N. Kumar, M.G. Angelos, H.M. Powell, et al., Sustained release of basic fibroblast growth factor (bFGF) encapsulated polycaprolactone (PCL) microspheres promote angiogenesis in vivo, Nanomaterials (Basel) 9 (7) (2019), https://doi.org/10.3390/nano9071037.
[35] A. Nouvong, A.M. Ambrus, E.R. Zhang, L. Hultman, H.A. Coller, Reactive oxygen species and bacterial biofilms in diabetic wound healing, Physiol Genomics 48 (12) (2016) 889–896, https://doi.org/10.1152/physiolgenomics.00066.2016.
[36] Y.F. Lu, H.S. Li, J. Wang, M.Y. Yao, Y. Peng, T.F. Liu, et al., Engineering bacteria-activated multifunctionalized hydrogel for promoting diabetic wound healing, Advanced Functional Materials 31 (48) (2021), https://doi.org/10.1002/adfm.202105749.
[37] Q.Y. Jia, Z. Fu, Y.S. Li, Z.J. Kang, Y.T. Wu, Z.Q. Ru, et al., Hydrogel loaded with peptide-containing nanocomplexes: symphonic cooperation of photothermal antimicrobial nanoparticles and prohealing peptides for the treatment of infected wounds, Acs Applied Materials & Interfaces 16 (11) (2024) 13422–13438, https://doi.org/10.1021/acsami.3c16061.
[38] Z. Fu, H.L. Sun, Y.T. Wu, C. Li, Y.L. Wang, Y.X. Liu, et al., A cyclic heptapeptide-based hydrogel boosts the healing of chronic skin wounds in diabetic mice and patients, Npg Asia Materials 14 (1) (2022), https://doi.org/10.1038/s41427-022-00444-x.
[39] P. Qin, J. Tang, D.D. Sun, Y. Yang, N.X. Liu, Y.L. Li, et al., Zn cross-linked alginate carrying hollow silica nanoparticles loaded with RL-QN15 peptides provides promising treatment for chronic skin wounds, Acs Applied Materials & Interfaces 14 (26) (2022) 29491–29505, https://doi.org/10.1021/acsami.2c03583.
[40] C.D. Zhang, X. Yang, L.D. Yu, X.S. Chen, J.K. Zhang, S. Zhang, et al., Electrospun polyasparthydrazide nanofibrous hydrogel loading with in-situ synthesized silver nanoparticles for full-thickness skin wound healing application, Materials & Design (2024) 239, https://doi.org/10.1016/j.matdes.2024.112818.
[41] Y.R. Li, W.W. Zhao, S.J. Chen, H.Y. Zhai, S.H. Wu, Bioactive electrospun nanoyarn-constructed textile dressing patches delivering Chinese herbal compound for accelerated diabetic wound healing, Materials & Design (2024) 237, https://doi.org/10.1016/j.matdes.2023.112623.
[42] Z. Pan, K.R. Zhang, H.L. Gao, Y. Zhou, B.B. Yan, C. Yang, et al., Activating proper inflammation for wound-healing acceleration via mesoporous silica nanoparticle tissue adhesive, Nano Research 13 (2) (2020) 373–379, https://doi.org/10.1007/s12274-020-2619-x.
[43] H. Ezhilarasu, D. Vishalli, S.T. Dheen, B.H. Bay, D.K. Srinivasan, Nanoparticle-based therapeutic approach for diabetic wound healing, Nanomaterials 10 (6) (2020), https://doi.org/10.3390/nano10061234.
[44] G.Y. Wang, W. Wang, Z.S. Chen, T. Hu, L.F. Tu, X.L. Wang, et al., Photothermal microneedle patch loaded with antimicrobial peptide/MnO2 hybrid nanoparticles for chronic wound healing, Chemical Engineering Journal 482 (2024), https://doi.org/10.1016/j.cej.2024.148938.
[45] T.W. Huang, Y.C. Ho, T.N. Tsai, C.L. Tseng, C. Lin, F.L. Mi, Enhancement of the permeability and activities of epigallocatechin gallate by quaternary ammonium chitosan/fucoidan nanoparticles, Carbohydrate Polymers 242 (2020), https://doi.org/10.1016/j.carbpol.2020.116312.
[46] S. Parcell, Sulfur in human nutrition and applications in medicine, Altern Med Rev 7 (1) (2002) 22–44.
[47] S. Shankar, R. Pangeni, J.W. Park, J.-W.J.M.S. Rhim, E. C, Preparation of Sulfur Nanoparticles and Their Antibacterial Activity and Cytotoxic Effect, vol. 92, 2018, pp. 508–517.
[48] J.A. Smith, R. Mulhall, S. Goodman, G. Fleming, H. Allison, R. Raval, et al., Investigating the antibacterial properties of inverse vulcanized sulfur polymers, Acs Omega 5 (10) (2020) 5229–5234, https://doi.org/10.1021/acsomega.9b04267.
[49] J.O. Russell, F.D. Camargo, Hippo signalling in the liver: role in development, regeneration and disease, Nat Rev Gastroenterol Hepatol 19 (5) (2022) 297–312, https://doi.org/10.1038/s41575-021-00571-w.
[50] A. Dey, X. Varelas, K.L. Guan, Targeting the Hippo pathway in cancer, fibrosis, wound healing and regenerative medicine, Nat Rev Drug Discov. 19 (7) (2020) 480–494, https://doi.org/10.1038/s41573-020-0070-z.
[51] M. Mustafa, J.Y. Winum, The importance of sulfur-containing motifs in drug design and discovery, Expert Opinion on Drug Discovery 17 (5) (2022) 501–512, https://doi.org/10.1080/17460441.2022.2044783.
[52] J.J. Zou, J.Q. Le, B.C. Zhang, M.Y. Yang, J.L. Jiang, J.F. Lin, et al., Accelerating transdermal delivery of insulin by ginsenoside nanoparticles with unique permeability, International Journal of Pharmaceutics 605 (2021).
[53] X.S. Wang, J.F. Ge, E.E. Tredget, Y.J. Wu, The mouse excisional wound splinting model, including applications for stem cell transplantation, Nature Protocols 8 (2) (2013) 302–309, https://doi.org/10.1038/nprot.2013.002.
[54] L. Maddaluno, C. Urwyler, S. Werner, Fibroblast growth factors: key players in regeneration and tissue repair, Development 144 (22) (2017) 4047–4060, https://doi.org/10.1242/dev.152587.
[55] H. Clevers, K.M. Loh, R. Nusse, Stem cell signaling. An integral program for tissue renewal and regeneration: wnt signaling and stem cell control, Science 346 (6205) (2014) 1248012, https://doi.org/10.1126/science.1248012.
[56] M. Fu, Y. Hu, T. Lan, K.L. Guan, T. Luo, M. Luo, The Hippo signalling pathway and its implications in human health and diseases, Signal Transduct Target Ther 7 (1) (2022) 376, https://doi.org/10.1038/s41392-022-01191-9.
[57] J. Gao, L. Fan, L. Zhao, Y. Su, The interaction of Notch and Wnt signaling pathways in vertebrate regeneration, Cell Regen 10 (1) (2021) 11, https://doi.org/10.1186/s13619-020-00072-2.
[58] Y. Zhang, P.A. Beachy, Cellular and molecular mechanisms of Hedgehog signalling, Nat Rev Mol Cell Biol 24 (9) (2023) 668–687, https://doi.org/10.1038/s41580-023-00591-1.
[59] B. Wang, Y. Huang, Z. Huang, H. Wang, J. Chen, X. Pan, et al., Self-assembling in situ gel based on lyotropic liquid crystals containing VEGF for tissue regeneration, Acta Biomater 99 (2019) 84–99, https://doi.org/10.1016/j.actbio.2019.09.011.
[60] K.D. Poss, J. Shen, A. Nechiporuk, G. McMahon, B. Thisse, C. Thisse, et al., Roles for Fgf signaling during zebrafish fin regeneration, Dev Biol 222 (2) (2000) 347–358, https://doi.org/10.1006/dbio.2000.9722.
[61] S.E. Riley, Y. Feng, C.G. Hansen, Hippo-Yap/Taz signalling in zebrafish regeneration, NPJ Regen Med 7 (1) (2022) 9, https://doi.org/10.1038/s41536-022-00209-8.
[62] N. Su, M. Jin, L. Chen, Role of FGF/FGFR signaling in skeletal development and homeostasis: learning from mouse models, Bone Res 2 (2014) 14003, https://doi.org/10.1038/boneres.2014.3.
[63] I. Mannaerts, S.B. Leite, S. Verhulst, S. Claerhout, N. Eysackers, L.F. Thoen, et al., The Hippo pathway effector YAP controls mouse hepatic stellate cell activation, J Hepatol 63 (3) (2015) 679–688, https://doi.org/10.1016/j.jhep.2015.04.011.

[64] K. Geng, X. Ma, Z. Jiang, W. Huang, C. Gao, Y. Pu, et al., Innate immunity in diabetic wound healing: focus on the mastermind hidden in chronic inflammatory, Front Pharmacol 12 (2021) 653940, https://doi.org/10.3389/fphar.2021.653940.
[65] S.K. Shukla, A.K. Sharma, V. Gupta, M.H. Yashavarddhan, Pharmacological control of inflammation in wound healing, J Tissue Viability 28 (4) (2019) 218–222, https://doi.org/10.1016/j.jtv.2019.09.002.
[66] A.E. Louiselle, S.M. Niemiec, C. Zgheib, K.W. Liechty, Macrophage polarization and diabetic wound healing, Transl Res 236 (2021) 109–116, https://doi.org/10.1016/j.trsl.2021.05.006.